Chaos, Solitons and Fractals 173 (2023) 113745

Contents lists available at ScienceDirect

Chaos, Solitons and Fractals

journal homepage: www.elsevier.com/locate/chaos

Coupled quantum pendula as a possible model for Josephson-junction-based axion detection

Roberto Grimaudo [a], Davide Valenti [a,*], Giovanni Filatrella [b], Bernardo Spagnolo [a,c], Claudio Guarcello [d,e]

[a] Dipartimento di Fisica e Chimica "Emilio Segrè", Group of Interdisciplinary Theoretical Physics, Università degli Studi di Palermo, Viale delle Scienze, Ed. 18, Palermo, I-90128, Sicily, Italy
[b] Dep. of Sciences and Technologies and Salerno unit of INFN, University of Sannio, Via Port'Arsa 11, Benevento, I-82100, Campania, Italy
[c] Lobachevskii University of Nizhnii Novgorod, 23 Gagarin Ave., Novgorod, 603950, Nizhnii, Russia
[d] Dipartimento di Fisica "E.R. Caianiello", Università di Salerno, Via Giovanni Paolo II 132, Fisciano (SA), I-84084, Campania, Italy
[e] INFN, Sezione di Napoli Gruppo Collegato di Salerno, Complesso Universitario di Monte S. Angelo, Napoli, I-80126, Campania, Italy

ARTICLE INFO

Keywords:
Coupled pendula
Axions
Josephson qubits
Resistively and Capacitively shunted junction model
thermal noise effects

ABSTRACT

The model of two coupled quantum pendula is studied and its suitability to describe Josephson junctions interacting with axions is analysed. It is shown that some physical features of one pendulum, not directly accessible, can be deduced by local measures on the other one, which is experimentally available. Such an effect can be exploited for the axion (the invisible pendulum) detection based on Josephson junctions (the accessible pendulum). The interaction between axion and Josephson junction can be enhanced at the resonance, if the axion and the junction frequencies match, and if the accessible system is prepared in the most convenient initial quantum state.

1. Introduction

Nonlinearity is ubiquitous in nature and can cause many intriguing dynamic effects. For example, the co-presence of nonlinear interactions and noise gives rise to counterintuitive effects, such as stochastic resonance [1–7], noise enhanced stability [8–10], and stochastic resonant activation [11–13]. Other scenarios where the role of nonlinearity and noise is fundamental in determining system dynamics can be found in memristive systems [14], and in biological and ecological systems [15–21]. In the vast realm of nonlinear dynamics, we focus on the study of coupled oscillators, looking in particular at the pendulum as an archetypal oscillator. Interacting oscillators, needless to say, have been exploited to describe a plethora of physical systems, since the discovery of synchronization of two heavy clocks by Huygens [22], which was extended to many oscillators [23] also to describe synchronization in biology [24] and many applications [25]. Interacting pendula are similar to two interacting Josephson junctions (JJs) [26,27] and, as recently proposed, can be used to describe the dynamics of a JJ coupled to axion particles [28]. The aim of the present work is to model the dynamics of two distinct coupled pendula, which differ not so much in their constitutive parameters, but rather in their accessibility, in the sense that we assume one (equivalent to a JJ) experimentally controllable and the other (equivalent to the axion field) inaccessible, but whose characteristics we would like to infer.

The relevance and the growing interest towards the axion search, both theoretical and experimental, is proved by the remarkable increase of works in the last years [29–42]. A wide class of experiments has been proposed in order to probe the presence of axions [43–51]. These experiments are based on the axion–photon conversion (Primakoff effect) in the presence of an external magnetic field, due to a coupling between axions and photons [52–54]. Recently, the interaction between a Josephson qubit and the axion-induced photons in a resonant cavity has been analysed [55].

Josephson junctions, modelled by a sinusoidal potential formally equivalent to a pendulum, are of paramount importance in many fields [56–61] and play a leading role in the search of possible protocols and schemes for the single-photon detection and the above mentioned axion search [62–70]. Among the detection methods proposed, Josephson-based experiments, based on a direct interaction between axions and JJs [28,71], may help to understand unclear "events" in the Josephson response [72–74]. However, in spite of the intense efforts, no direct observations have been registered in terrestrial controlled experiments up to date.

* Corresponding author at: Dipartimento di Fisica e Chimica "Emilio Segrè", Group of Interdisciplinary Theoretical Physics, Università degli Studi di Palermo, Viale delle Scienze, Ed. 18, Palermo, I-90128, Sicily, Italy.
E-mail address: davide.valenti@unipa.it (D. Valenti).

https://doi.org/10.1016/j.chaos.2023.113745
Received 25 May 2023; Accepted 19 June 2023
Available online 10 July 2023

In the present work, by exploiting the nonlinearity of the two coupled differential equations and considering appropriate physical conditions, we formally quantize the model of the two pendula. In this way, a mathematical framework describing two interacting effective two-level systems (TLS) is considered [75]. Within this description the dynamics of one pendulum is influenced by the presence of the other. If we suppose that only one of the two subsystems can be experimentally addressed, we demonstrate that, by measuring appropriate physical quantities of this *accessible pendulum* (AP), it is possible not only to reveal the presence of the *dark pendulum* (DP), but also to evaluate the interaction strength between the two subsystems. The main signature of the DP presence is the occurrence of induced oscillations in the AP, due to the resonant frequency-matching between the two subsystems.

Although we discuss the possibility to exploit this effect for a proposal of a Josephson-based axion detection, here we will not delve deeper into the details of the cosmological problem, but we just deal with the study of two coupled pendula dynamics. However, in possible applications a quantum description of the axion as an effective TLS (appropriated in environments characterized by negligible noise) is required. The quantized version of the axion as an effective TLS can be justified in analogy with the Josephson systems. Since, under specific conditions, JJs actually behave as TLSs [75,76], it is possible to assume that, if similar conditions are satisfied by the axion field, the latter shares the same nonlinearity and hence the same quantum description can be suitable for the axion.

2. Two coupled pendula

Let us consider the following system of differential equations

$$\ddot{\varphi} + a_1\dot{\varphi} + b_1 \sin(\varphi) = \gamma(\ddot{\theta} - \ddot{\varphi}), \tag{1a}$$

$$\ddot{\theta} + a_2\dot{\theta} + b_2 \sin(\theta) = \gamma(\ddot{\varphi} - \ddot{\theta}), \tag{1b}$$

that describe two coupled pendula. Here, (a_1, a_2) and (b_1, b_2) are the dissipation and frequency parameters, respectively [13]; γ is the coupling constant between the two systems. The mathematical model of coupled pendula also describes the dynamics of two capacitively-coupled JJs [26,27], and the possible coupling mechanism between a JJ and an axion particle [28] (see Appendix A for more details).

2.1. Fully quantized model

It is well known that an ideal physical system described by each of the two equations can be formally identified with a particle (point-like) moving in a *cosine* potential (see Appendix A). One can suppose the existence of quantized levels within each well of the potential. The levels are not equally spaced because of the nonlinearity of the *cosine* potential. Therefore, under specific physical conditions, such as low noise and low temperature, the dynamics can be restricted to just the two lowest levels [75] and the system described by the two coupled differential equations amounts to two interacting quantum TLSs. The quantum Hamiltonian, in unit of $\hbar$, can be cast as follows [75]

$$H_{ADP} = \omega_{AP}\hat{\sigma}^z_{AP} + \omega_{DP}\hat{\sigma}^z_{DP} + \gamma\hat{\sigma}^x_{AP}\hat{\sigma}^x_{DP}. \tag{2}$$

The above Hamiltonian model can be used to study, for example, two spin-1/2 subjected to two local effective fields (ω_{AP} and ω_{DP}) and coupled through the simpler Heisenberg interaction of strength γ [77].

2.2. Induced oscillations

The dynamical problem related to Eq. (2) can be exactly solved; the energy spectrum and the time evolution operator can be analytically derived. The symmetry property of the Hamiltonian H_{ADP} allows to reduce the system dynamics to that of two independent TLSs. In other words, the existence of a constant of motion generates two dynamically invariant two-dimensional subspaces, within which the system can be effectively described in terms of a single TLS. In this way the solution of two effective independent two-level dynamics solves the dynamics of the original system of two coupled quantum pendula (see Appendix B).

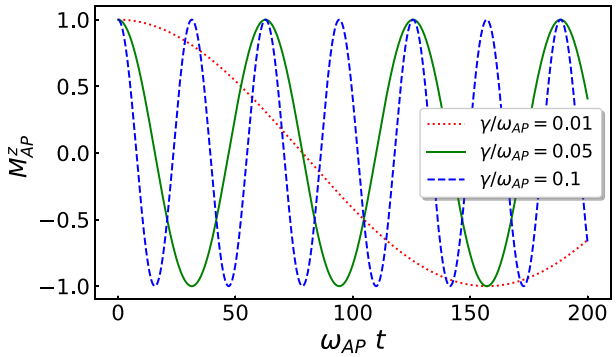

Fig. 1. Oscillations of the magnetization M^z_{AP} of the addressable pendulum induced by the dark one when the other starts from $\rho_{AP}(0) = |+\rangle\langle+|$ and for three different values of γ/ω_{AP}: 0.01 (dotted red line), 0.05 (full green line), 0.1 (dashed blue line). (For interpretation of the references to colour in this figure legend, the reader is referred to the web version of this article.)

Of course, if the condition $k_BT \ll \omega_{AP}$ is satisfied and the coupling between the subsystems is zero ($\gamma = 0$), the AP would remain in its initial state. Conversely, if $\gamma \neq 0$, transitions might occur for the presence of the DP. Therefore, clear signatures of the presence of the second system can be detected through local measures on the first system. Let us assume that the AP is prepared in the state $\rho_{AP} = |-\rangle\langle-|$, $(\hat{\sigma}^z|\pm\rangle = \pm|\pm\rangle)$, while the second one in a generic classical mixture

$$\rho_{DP} = p\ |+\rangle\langle+| + (1-p)|-\rangle\langle-|, \tag{3}$$

with $p \in [0,1]$. In this case, the population $\rho^{11}_{AP}(t) = \langle+|\rho_{AP}(t)|+\rangle$, in the limit $\gamma \ll \omega_{AP}, \omega_{DP}$ and for $\omega_{AP} \simeq \omega_{DP}$, varies over the time as (see Appendix B)

$$\rho^{11}_{AP}(t) = p\ \sin^2(\gamma t), \tag{4}$$

and the 'magnetization' $M^z_{AP}(t) \equiv \mathrm{Tr}\{\rho_{AP}(t)\hat{\sigma}^z_{AP}\}$ of the AP is given by

$$M^z_{AP}(t) = 2p\sin^2(\gamma t) - 1. \tag{5}$$

In the prescribed limits, the oscillations induced in the AP clearly emerge and can be exploited to detect the presence of the DP. Furthermore, the frequency that characterizes such oscillations is, and more in general depends on, the coupling parameter. For this reason, by analysing the characteristic period of such a peculiar, periodically oscillating behaviour of the AP, the estimate of γ can be deduced. Analogous results are obtained for a generic quantum state ($|\psi_a\rangle = \alpha|+\rangle + \beta|-\rangle$, $|\alpha|^2 + |\beta|^2 = 1$) of the DP (see Appendix B).

The condition $\omega_{AP} \simeq \omega_{DP}$ is essential for the oscillations to occur more clearly. In general, in fact, the expression of $\rho^{11}_{AP}(t)$ is slightly more complicated, since several contributions with different amplitudes and frequencies are present [see Eqs. (B.22)]. Since, by hypothesis, $\gamma \ll \omega_{AP}, \omega_{DP}$, if $\omega_{AP} \neq \omega_{DP}$ the oscillations are tamed and practically impossible to observe, since all the contributions are negligible. In the resonance condition, instead, there is a term that gives a non-zero contribution (see Appendix B). Therefore, the matching between the frequencies of the two systems is the basic condition for the DP to induce a detectable dynamics of the AP.

Moreover, it should be noted that at finite temperatures, that is including thermally activated states with probability $p = 1/\left[1 + \exp\left(\omega_{DP}/k_BT\right)\right]$, the condition $\omega_{DP} \gg k_BT$ implies $p \approx 0$, and the DP is in its down state $\rho_{DP} = |-\rangle\langle-|$. This is reasonable since, at very low temperatures, thermal transitions are forbidden and the DP has an overwhelming probability of being in its down state. The condition $\gamma \ll \omega_{AP}, \omega_{DP}$ freezes the two systems in their initial state, and any

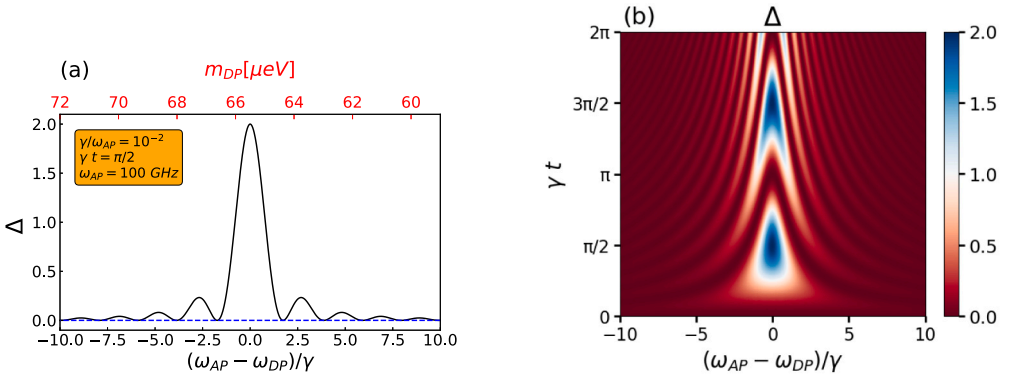

Fig. 2. (a) The amplitude $\Delta \equiv \max(M^z_{AP}) - \min(M^z_{AP})$ of the oscillations as a function of the frequency difference $\omega_{AP} - \omega_{DP}$ for the same initial condition of Fig. 1 [$M^z_{AP}(t = 0) = 1$], and at the fixed time-instant $t = \pi/2\gamma$; the top x-axis refers to the axion-mass values swept in the considered range of frequencies when $\omega_{AP} = 100$ GHz. (b) The amplitude Δ plotted in the phase space region $\{\gamma\, t;\ (\omega_{AP} - \omega_{DP})/\gamma\}$. The resonant condition is clearly visible at $\omega_{DP} = \omega_{AP}$. Here, for $\gamma\, t = (2k + 1)\pi/2,\ k \in \mathrm{N}$, the transition of the addressable pendulum from the up- to the down-state occurs more clearly.

measurable observable does not change. To avoid this problem, it is more convenient to initially prepare the AP in the up-state $\rho_{AP}(0) = |+\rangle\langle+|$. The conditions $\omega_{AP} \simeq \omega_{DP}$ and $p \approx 0$ imply (see Appendix B)

$$\rho^{11}_{AP}(t) = \cos^2(\gamma t)\,, \tag{6}$$

and consequently the magnetization

$$M^z_{AP}(t) = \cos(2\gamma t) \tag{7}$$

presents a periodic reversal phenomenon, shown in Fig. 1 for three different values of γ. Therefore, in addition to the synchronization regime ($\omega_{AP} \simeq \omega_{DP}$), the initial state of the AP is also essential to enhance the oscillations induced by the DP.

According to Eqs. (B.25), the amplitude $\Delta \equiv \max(M^z_{AP}) - \min(M^z_{AP})$ of the oscillations induced in the magnetization of the JJ (the AP) at the fixed time-instant $t = \pi/2\gamma$ is shown in Fig. 2(a) as a function of the frequency difference $\omega_{AP} - \omega_{DP}$. The peak at $\omega_{AP} = \omega_{DP}$ in this plot can be interpreted as a resonance effect, which arises if one fixes the AP frequency ω_{AP}, and modifies the DP frequency ω_{DP}, by varying the mass across the possible range of values.

3. Possible application for Josephson-based axion detection

In this section the utility of the previous results is illustrated in the framework of Josephson-based axion detection, where JJ and axion play the role of AP and DP, respectively.

On the basis of the highlighted result and in the ideal scheme previously outlined, through appropriate experimental tests and investigations on the JJ, it might be possible, in principle, to reveal the presence of the axionic dark matter. Indeed, if the axion–JJ coupling is different from zero and the physical conditions considered (low noise and temperature) for the two subsystems (JJ and axion) are valid, the measurable induced oscillations on the JJ could probe the presence of the axion field.

As shown in Fig. 2(a), this effect should be maximum when the axion and JJ frequencies are very close. It is interesting to note that resonance conditions arise also in other contexts [13,28] as a fundamental constraint for the emergence of axion-induced phenomena in Josephson systems. In the top x-axis of Fig. 2(a) the axion-mass values, swept in the considered range of frequencies when the Josephson frequency is $\omega_{AP} \equiv \omega_J = 100$ GHz, are shown. The value of ω_J is within the supposed axion-frequency range given in Eq. (A.8), with $\omega_{DP} \equiv \omega_a$. The same quantity Δ is plotted in Fig. 2(b) in the phase space $\{\gamma\, t;\ (\omega_J - \omega_a)/\gamma\}$. The resonant condition due to the Josephson-axion frequency matching is clearly visible at $\gamma\, t = (2k + 1)\pi/2,\ k \in \mathrm{N}$, where the transition of the JJ from its initial up-state to the down-state occurs.

This resonant dynamical regime reveals a detectable axion-induced dynamics in the JJ, and can be exploited for axion detection. In fact, one can possibly think of an array of JJs with different plasma frequencies, which is obtainable through an appropriate change of critical currents and/or capacitances of the junctions. To span mass values in the range [10 μeV−1 meV], it is possible to fabricate an array of JJs tuned to several corresponding frequency values: 10 GHz $< \omega_J <$ 1 THz, which is a realistic range for JJs. Quantitatively, the analysis of the sensitivity, defined as the width of the peak at $1/e$ (with e the Nepero number) of the magnetization amplitude and entailed by Fig. 2(a), gives $\pm 0.95\,\mu$eV. Thus, an array of about 500 JJs covers the whole range of mass values, exploiting a modulation of the junction parameters that is similar, for example, to that proposed, in another context, in Ref. [78]. In mechanical terms, one can imagine 500 pendula of different lengths, each coupled to a dark and unknown pendulum whose features have being sought. If the dark pendulum exists, it swings (in quantum terms, switches from a state to another) the accessible pendulum, whose length determines the tuning to the dark one.

4. Conclusions

In this work we have considered the mathematical model of two coupled pendula. At very low temperatures, each pendulum should dynamically behave as an effective TLS. We have supposed the condition where one pendulum is experimentally accessible, while the other, the "dark" pendulum, is not accessible. By solving exactly the dynamic problem, we have demonstrated the existence of oscillations induced on the accessible pendulum by the dark pendulum. In this way we have highlighted that, through measurements on the accessible pendulum, the presence, as well as the characteristics, of the dark pendulum could be derived.

We have shown how such a result could underlie an ideal experimental scheme for axion detection using JJs. The classical model of the two coupled pendula has been proposed to describe a JJ interacting with an axion particle [28]. The close analogy between the axion–JJ system and two coupled JJs allows exploiting the qubit–qubit Hamiltonian to describe the axion–JJ system as two interacting TLSs (under specific conditions, i.e. low noise and temperature). In this context, the JJ (the axion) plays the role of the accessible (dark) pendulum, and one can speak of axion-induced oscillations in the JJ.

Such oscillations can be enhanced by suitably preparing the Josephson qubit in its up-state, and matching the Josephson frequency ω_J with the axion frequency ω_a (synchronization regime). Furthermore, the last condition makes the oscillation frequency linearly dependent on the axion–JJ coupling. The assumption of a reasonable very low axion–JJ coupling requires long-term experimental investigations. Given the

typical duration of experiments based on Josephson-qubit [75,76], one could hypothesize that a possible cause of the lack of traces of the axion-induced oscillations is the limited stability of the experiments conducted so far. Therefore, long-term experiments, in the quantum limit of low noise and weak coupling with the environment, can be aimed at the identification of JJ oscillations, and at the same time they could reveal the presence of axion particles and provide information about the axion–JJ coupling parameter.

Declaration of competing interest

The authors declare that they have no known competing financial interests or personal relationships that could have appeared to influence the work reported in this paper.

Data availability

No data was used for the research described in the article.

Acknowledgments

RG acknowledges support by the PRIN Project PRJ-0232 - Impact of Climate Change on the biogeochemistry of Contaminants in the Mediterranean sea (ICCC). GF acknowledges support by Italian Institute of Nuclear Physics (INFN) through the DARTWARS project. BS acknowledges support by Government of the Russian Federation through Agreement No. 074-02-2018-330 (2). All the authors acknowledge the support of the Ministry of University and Research of Italian Government.

Appendix A. Josephson junctions and axions

A.1. Josephson junctions

The dynamics of the Josephson phase φ can be described with the resistively and capacitively shunted junction (RCSJ) model [11,12,79–83],

$$\frac{d^2\varphi}{dt^2} + \frac{1}{RC}\frac{d\varphi}{dt} + \frac{2\pi}{\Phi_0}\frac{I_c}{C}\sin[\varphi(t)] = 0. \tag{A.1}$$

Here, I_c is the maximum Josephson current that can flow through the device, and R and C are the normal-state resistance and capacitance of the JJ, respectively. $\Phi_0 = h/2e$ is the superconducting magnetic flux quantum, with e the electron charge.

The quantum Hamiltonian of a JJ can be written as

$$H = 4E_c\hat{n}^2 - E_J\cos(\hat{\varphi}), \tag{A.2}$$

where $\hat{n}$ and $\hat{\varphi}$ represent the charge and phase non-commuting operators, respectively, while $E_c = e^2/2C$ and $E_J = I_c\Phi_0/2\pi$. If $E_J \gg E_c$ ($E_J \ll E_c$), the phase (charge) is a 'good' quantum number, that is the phase (charge) has a precise value, while the charge (phase) is completely undetermined. Under the conditions $E_J \gg E_c$ and $E_J \gg k_BT$ (k_B being the Boltzmann and T the temperature), the JJ effectively behaves like a TLS (qubit) and thus it can be formally described in terms of spin-1/2 dynamical variables [75,76]. This is possible thanks to the characteristic anharmonicity of the Josephson systems stemming from the sinusoidal term in Eq. (A.2). The Hamiltonian of the effective qubit system, called phase qubit, reads

$$H_J = \hbar\omega_J\hat{\sigma}_J^z, \tag{A.3}$$

where $\hbar$ is the reduced Planck constant, $\hat{\sigma}_J^z$ is the well known spin-1/2 Pauli operator, and $\omega_J = (\sqrt{8E_JE_c} - E_c)/\hbar = \omega_p - E_c/\hbar$ is the effective qubit frequency. The latter comes from the Lamb-shift-induced correction $E_c/\hbar$ to the plasma frequency $\omega_p = \sqrt{8E_JE_c}/\hbar$.

If $E_J \ll E_c$, the Josephson dynamics is analogous to that of a TLS, and a charge-qubit is generated. However, in this regime, the effective qubit system becomes highly sensitive to the charge noise, which is more challenging to be reduced than the flux noise.

A.2. Axions

The axion field is $a = f_a\theta$, where f_a and θ are the axion coupling constant and the misalignment angle, respectively. Within the Robertson–Walker metric, which is appropriate to describe the early universe, the equation of motion of $\theta(t) = a(t)/f_a$ reads [34]

$$\frac{d^2\theta(t)}{dt^2} + 3H\frac{d\theta(t)}{dt} + \frac{m_a^2c^4}{\hbar^2}\sin[\theta(t)] = 0, \tag{A.4}$$

where spatial gradients are neglected [13]. Here, $H \approx 2\times10^{-18}\ s^{-1}$ is the Hubble parameter and m_a denotes the axion mass. The typical ranges of parameters that are allowed for dark matter axions are [84,85]

$$3\times10^9\ \text{GeV} \le f_a \le 10^{12}\ \text{GeV}. \tag{A.5}$$

and

$$6\times10^{-6}\ \text{eV} \le m_ac^2 \le 2\times10^{-3}\ \text{eV}. \tag{A.6}$$

The forcing term $\sin(\theta)$ is due to quantum chromodynamics instanton effects. The effective axion potential is defined as

$$V(\theta) = \frac{m_a^2c^4}{\hbar^2}(1-\cos\theta). \tag{A.7}$$

The misalignment mechanism explains the emergence of the axion mass as due to the initial non-equilibrium position [$\theta(0) \neq 0$], which induces oscillations of the axions around the potential minimum [34]. The axion, therefore, can be effectively described as a particle in an anharmonic potential well, whose anharmonicity stems from the $\cos(\theta)$ term, implying that for small oscillations [$V(\theta) \propto m_a\theta^2/2$] the axion dynamics is analogous to that of a harmonic oscillator. This effective dynamic description is analogous to that of a JJ, since the analytical form of the potential is the same. Further, the similarity between the axion field and the JJ equation is evident: the axion dynamics is analogous to that of an RCSJ with no externally applied bias current. Moreover, it is worth to remark that, besides the formal mathematical analogy between the two systems, the normalized parameters characterizing the two equations are quite similar as their order of magnitude is concerned [13]. As for JJs, the axion degrees of freedom can be quantized. In this framework, therefore, it can be argued that the anharmonicity of the *cosine* term induces a nonconstant spacing of the quantized energy levels in the potential well.

In the light of the previous observation, by comparing the axion equation with that of the JJ and by establishing a correspondence between the analogous terms, it is possible to verify that the axion can be regarded as a JJ characterized by a plasma frequency within the range

$$m_ac^2/\hbar \equiv \omega_a \in [9,\ 3\cdot10^3]\,\text{GHz}, \tag{A.8}$$

which is close to the typical values of the Josephson plasma frequencies. This frequency, both for the axion and the JJ, corresponds to the frequency of small oscillations at the bottom of a well of the *cosine* potential. Based on this analogy, in the low-temperature regime $\hbar\omega_a \gg k_BT$, one can suppose that also the axion can be approximately considered as a TLS, restricting to the two lowest quantized levels of the system, with the following effective Hamiltonian

$$H_a = \hbar\omega_a\hat{\sigma}_a^z, \tag{A.9}$$

where $\hat{\sigma}_a^z$ is the Pauli operator associated to the axion.

A.3. Axion-JJ system

Several paradigms to search and detect axionic dark matter in the halo of our galaxy are based on the coupling between axion and photon [13,54,86]. In analogy to what happens in resonant cavities, the decay of the axion in photons is supposed to be responsible for the

axion–JJ coupling. The axion–JJ interaction was assumed in Ref. [28] to be formally written as

$$\ddot{\varphi} + a_1\dot{\varphi} + b_1 \sin(\varphi) = \gamma(\ddot{\theta} - \ddot{\varphi}), \tag{A.10a}$$

$$\ddot{\theta} + a_2\dot{\theta} + b_2 \sin(\theta) = \gamma(\ddot{\varphi} - \ddot{\theta}), \tag{A.10b}$$

where (a_1, a_2) and (b_1, b_2) are the dissipation and frequency parameters, respectively [13]; γ is the coupling constant between the two systems and its value can be inferred from experimental quantities. This proposal is based on the fact that the axion differential equation is analogous to that of a JJ and then the axion particle can be dynamically seen by the JJ as another fictional JJ. The physical origin of such a supposed coupling can be ascribed to the fact that the axion, entering the JJ, decays near the surface into two photons (Primakoff effect), one of which (that with vanishing momentum) generates an electron–hole pair which, in turn, after Andreev reflections, gives rise to a detectable current. Furthermore, the axion–JJ coupling is correlated only with the axion–JJ synchronization and the probability that the axion decays into photons, regardless of the strength of the axion–photon coupling. Therefore, an experimental setup constituted of JJ-based axion detectors, according to the present approach, can only give information about the axion mass and the axion–JJ coupling, and not about the axion–photon coupling parameter.

Appendix B. Coupled quantum pendula and their dynamics

Let us consider the following model (in units of $\hbar$)

$$H = \omega_J\hat{\sigma}_J^z + \omega_a\hat{\sigma}_a^z + \gamma\hat{\sigma}_J^x\hat{\sigma}_a^x, \tag{B.1}$$

describing two interacting TLSs subject to two local longitudinal (along the z direction) fields (ω_1 and ω_2). Here, $\hat{\sigma}_i^x$ and $\hat{\sigma}_i^z$ ($i = 1, 2$) are the Pauli matrices.

The Hamiltonian exhibits the following canonical symmetry transformation, that is it remains unchanged under such a transformation [77,87–90],

$$\hat{\sigma}_i^x \to -\hat{\sigma}_i^x, \quad \hat{\sigma}_i^z \to \hat{\sigma}_i^z, \quad i = J, a. \tag{B.2}$$

This fact implies the existence of a unitary time-independent operator, by construction a constant of motion, accomplishing the transformation (B.2). This unitary operator is given by $\pm\hat{\sigma}_J^z\hat{\sigma}_a^z$, being the transformation (B.2) nothing but the rotations of π around the $\hat{z}$ axis with respect to each spin, and reads

$$e^{i\pi\hat{S}_1^z/\hbar} \otimes e^{i\pi\hat{S}_2^z/\hbar} = -\hat{\sigma}_J^z\hat{\sigma}_a^z = \cos\left(\frac{\pi}{2}\hat{\Sigma}_z\right), \tag{B.3}$$

where $\hat{\Sigma}_z \equiv \hat{\sigma}_J^z + \sigma_a^z$. Eq. (B.3) shows that the constant of motion $\hat{\sigma}_J^z\hat{\sigma}_a^z$ is indeed a $\hat{\Sigma}_z$-based parity operator since, in correspondence of its integer eigenvalues $M = +2, 0, 0, -2$, it has eigenvalues $1, -1, -1, 1$, respectively. This constant of motion implies two dynamically invariant sub-dynamics related to the two eigenvalues of $\hat{\sigma}_J^z\hat{\sigma}_a^z$. We can extract these two sub-dynamics by considering that the operator $\hat{\sigma}_J^z\hat{\sigma}_a^z$ has the same spectrum as $\hat{\sigma}_a^z$, i.e., the same eigenvalues (±1) with the same twofold degeneracy. There exists therefore a unitary time-independent operator $\mathbb{U}$ transforming $\hat{\sigma}_J^z\hat{\sigma}_a^z$ in $\hat{\sigma}_a^z$. It can be easily seen that the unitary and Hermitian operator

$$T = \frac{1}{2}\left[\hat{1} + \hat{\sigma}_J^z + \hat{\sigma}_a^x - \hat{\sigma}_J^z\hat{\sigma}_a^x\right] \tag{B.4}$$

accomplishes the desired transformation

$$T^\dagger\hat{\sigma}_J^z\hat{\sigma}_a^z T = T\hat{\sigma}_J^z\hat{\sigma}_a^z T = \hat{\sigma}_a^z. \tag{B.5}$$

Transforming H into $\tilde{H} = T^\dagger H T$, we get

$$\tilde{H} = \omega_J\hat{\sigma}_J^z + \omega_a\hat{\sigma}_J^z\hat{\sigma}_a^z + \gamma\hat{\sigma}_J^x. \tag{B.6}$$

Therefore $\hat{\sigma}_a^z$ is a constant of motion of $\tilde{H}$ and, consequently, $\tilde{H}$ may be written parametrically in σ_a^z, by considering $\hat{\sigma}_a^z$ as a parameter

$$H_{\sigma_a^z} = \left(\omega_J + \omega_a\sigma_a^z\right)\hat{\sigma}_J^z + \gamma\hat{\sigma}_J^x. \tag{B.7}$$

That is, there exists two ($\sigma_a^z = \pm1$) two-dimensional sub-dynamics related to the two dynamically invariant Hilbert subspaces. The two-spin system, thus, in each dynamically invariant subspace behaves effectively as a TLS.

However, it is worth pointing out that the latter Hamiltonian is a four-dimensional Hamiltonian, since the operators of the first spin are to be understood as multiplied by the identity operator of the second spin (σ_a^z is just a number). Moreover, we can write two two-dimensional Hamiltonians of a fictitious TLS. In particular, when $\sigma_a^z = \pm1$, we get

$$H_\pm = \left(\omega_J \pm \omega_a\right)\hat{\sigma}^z + \gamma\hat{\sigma}^x. \tag{B.8}$$

These two Hamiltonians must be understood as effective two-dimensional Hamiltonians that govern the dynamics of the two-spin system within each dynamically invariant two-dimensional Hilbert subspace relative to one of the two eigenvalues of $\hat{\sigma}_a^z$. The overall dynamics of the two-spin system, therefore, in each subspace is equivalent to that of a fictitious single spin-1/2 immersed in a fictitious field.

In particular, the subspace related to the eigenvalue $+1$ of $\hat{\sigma}_a^z$ is spanned by the two-spin states $\{|{+}{+}\rangle, |{-}{-}\rangle\}$ ($\hat{\sigma}^z|\pm\rangle = \pm|\pm\rangle$) and the dynamics is ruled by the effective Hamiltonian H_+. Therefore, the two states $\{|{+}{+}\rangle, |{-}{-}\rangle\}$ are mapped into the states $\{|+\rangle, |-\rangle\}$ of the fictitious TLS. It follows that, in this case, by studying the dynamics of the fictitious TLS, we study the dynamics of the TLS within the space spanned by $\{|{+}{+}\rangle, |{-}{-}\rangle\}$. Analogously, the subspace related to the eigenvalue -1 of $\hat{\sigma}_a^z$ is spanned by the two-spin states $\{|{+}{-}\rangle, |{-}{+}\rangle\}$ and the effective two-level Hamiltonian, ruling the dynamics, is given by H_-. In this case, the two states $\{|+\rangle, |-\rangle\}$ of the fictitious spin-1/2 are the mapping images of the two two-spin states $\{|{+}{-}\rangle, |{-}{+}\rangle\}$.

It is important to point out that, even if we describe the dynamics within each subspace in terms of a single fictitious spin-1/2, it does not mean that the two actual TLSs are effectively decoupled. Actually, the dynamics within each subspace involves both the real spins; this can be easily seen by the fact that the spin states involved in each dynamically invariant subspace are two-spin states: $\{|{+}{+}\rangle, |{-}{-}\rangle\}$ in a subspace and $\{|{+}{-}\rangle, |{-}{+}\rangle\}$ in the other.

Let us consider the two two-dimensional Hamiltonians

$$H_\pm = \begin{pmatrix} \Omega_\pm & \gamma \\ \gamma & -\Omega_\pm \end{pmatrix}, \tag{B.9}$$

where $\Omega_\pm = \omega_J \pm \omega_a$. Each Hamiltonian represents a spin-1/2 or, more in general, a TLS subject to two time-dependent magnetic fields: one along the z-direction [giving rise to the energy term $\hbar\Omega(t)$], the other along the x-direction [giving rise to the energy term $\hbar\gamma(t)$]. It is important to point out that, in the two-level representation, what we call transverse field (along the x-direction) represents the coupling between the two real interacting spins. The solution of each (sub)dynamical problem is related to the solution of the Schrödinger equation $i\dot{U}_\pm = H_\pm U_\pm$ with $U_\pm(0) = 1$. Here, $U_\pm$ are the time evolution operators generated by $H_\pm$, and can be represented as

$$U_\pm(t) = \begin{pmatrix} a_\pm(t) & b_\pm(t) \\ -b_\pm^*(t) & a_\pm^*(t) \end{pmatrix}, \quad |a_\pm|^2(t) + |b_\pm|^2(t) = 1, \tag{B.10}$$

where $a_\pm(t)$ and $b_\pm(t)$ are two complex-valued functions whose expressions can be determined by solving the Schrödinger equation. The time evolution operator related to the two-spin Hamiltonian, represented in the coupled basis, takes the form

$$U(t) = \begin{pmatrix} a_+(t) & 0 & 0 & b_+(t) \\ 0 & a_-(t) & b_-(t) & 0 \\ 0 & -b_-^*(t) & a_-^*(t) & 0 \\ -b_+^*(t) & 0 & 0 & a_+^*(t) \end{pmatrix}. \tag{B.11}$$

It is straightforward to retrieve the two exact expressions of $a_\pm(t)$ and $b_\pm(t)$, that read

$$a_\pm(t) = \left[\cos\left(\nu_\pm t\right) - i\frac{\Omega_\pm}{\nu_\pm}\sin\left(\nu_\pm t\right)\right], \tag{B.12a}$$

$$b_{\pm}(t) = -i\frac{\gamma}{\nu_{\pm}}\sin\left(\nu_{\pm}t\right), \tag{B.12b}$$

with $\nu_{\pm} = \sqrt{\Omega_{\pm}^2 + \gamma^2}$.

If the two real spins are initialized in $|{-}{-}\rangle$, that is

$$\rho_{Ja}(0) = \begin{pmatrix} 0 & 0 & 0 & 0 \\ 0 & 0 & 0 & 0 \\ 0 & 0 & 0 & 0 \\ 0 & 0 & 0 & 1 \end{pmatrix}, \tag{B.13}$$

the dynamics of the two-spin system is restricted to the two-dimensional subspace spanned by $\{|{+}{+}\rangle, |{-}{-}\rangle\}$ and then only the solution of the dynamical problem related to H_+ is required. In this case, the initial state of the effective TLS, according to the underlying mapping, is $\rho_+(0) = |-\rangle\langle -|$. Therefore, the entries of the matrix

$$\rho_+(t) = U_+(t)\rho_+(0)U_+^{\dagger}(t) = \begin{pmatrix} \rho_{11}^+(t) & \rho_{12}^+(t) \\ \rho_{21}^+(t) & \rho_{22}^+(t) \end{pmatrix} \tag{B.14}$$

are exactly the four entries of the two-(real)spin matrix

$$\rho_{Ja}(t) = U(t)\rho_{Ja}(0)U^{\dagger}(t) = \begin{pmatrix} \rho_{11}^+(t) & 0 & 0 & \rho_{12}^+(t) \\ 0 & 0 & 0 & 0 \\ 0 & 0 & 0 & 0 \\ \rho_{21}^+(t) & 0 & 0 & \rho_{22}^+(t) \end{pmatrix}. \tag{B.15}$$

Of course, an analogous result is obtained if the two spins start from $|{-}{+}\rangle$. This implies that only the subdynamics governed by H_- is involved and then, on the basis of the mapping, we get the following evolved density matrix

$$\rho_{Ja}(t) = U(t)\rho_{Ja}(0)U^{\dagger}(t) = \begin{pmatrix} 0 & 0 & 0 & 0 \\ 0 & \rho_{11}^-(t) & \rho_{12}^-(t) & 0 \\ 0 & \rho_{21}^-(t) & \rho_{22}^-(t) & 0 \\ 0 & 0 & 0 & 0 \end{pmatrix}, \tag{B.16}$$

where the entries are those of the effective two-dimensional state $\rho_-(t) = U_-(t)\rho_-(0)U_-^{\dagger}(t)$.

Therefore, if the two spins start from the state

$$\rho_{Ja}(0) = \begin{pmatrix} 0 & 0 & 0 & 0 \\ 0 & 0 & 0 & 0 \\ 0 & 0 & |\alpha|^2 & \alpha\beta^* \\ 0 & 0 & \alpha^*\beta & |\beta|^2 \end{pmatrix} = \rho_J(0)\otimes\rho_a(0), \tag{B.17}$$

with

$$\begin{aligned} \rho_J(0) &= \begin{pmatrix} 0 & 0 \\ 0 & 1 \end{pmatrix} = |-\rangle\langle -|, \\ \rho_a(0) &= \begin{pmatrix} |\alpha|^2 & \alpha\beta^* \\ \alpha^*\beta & |\beta|^2 \end{pmatrix} = |\psi_a\rangle\langle\psi_a|, \quad |\psi_a\rangle = \alpha|+\rangle + \beta|-\rangle, \\ & |\alpha|^2 + |\beta|^2 = 1, \end{aligned} \tag{B.18}$$

one gets

$$\begin{aligned} \rho_J(t) &= \mathrm{Tr}_a\{\rho_{Ja}(t)\} \\ &= (|b_+|^2|\beta|^2 + |b_-|^2|\alpha|^2)|+\rangle\langle +| + \\ &\quad -(b_+a_-^*\alpha^*\beta + a_+^*b_-\alpha\beta^*)|+\rangle\langle -| + \\ &\quad -(b_+^*a_-\alpha\beta^* + a_+b_-^*\alpha^*\beta)|-\rangle\langle +| + \\ &\quad +(|a_+|^2|\beta|^2 + |a_-|^2|\alpha|^2)|-\rangle\langle -|. \end{aligned} \tag{B.19}$$

If, on the other hand, the initial state $\rho_{Ja}(0) = \rho_J(0)\otimes\rho_a(0)$ of the two spins is defined by

$$\begin{aligned} \rho_J(0) &= \begin{pmatrix} 0 & 0 \\ 0 & 1 \end{pmatrix} = |-\rangle\langle -|, \\ \rho_a(0) &= \begin{pmatrix} p & 0 \\ 0 & 1-p \end{pmatrix} = p\ |+\rangle\langle +| + (1-p)|-\rangle\langle -|, \\ & p \in [0,1] \end{aligned} \tag{B.20}$$

the reduced density matrix of the first spin becomes

$$\begin{aligned} \rho_J(t) &= \mathrm{Tr}_a\{\rho_{Ja}(t)\} \\ &= [(1-p)|b_+|^2 + p|b_-|^2]|+\rangle\langle +| + \\ &\quad +[(1-p)|a_+|^2 + p|a_-|^2]|-\rangle\langle -|. \end{aligned} \tag{B.21}$$

The probability $\rho_J^{11}(t) \equiv \langle +|\rho_J(t)|+\rangle$ of the transition $|-\rangle \to |+\rangle$ for the JJ thus reads

$$\rho_J^{11}(t) = (1-p)|b_+|^2 + p|b_-|^2, \tag{B.22a}$$

$$|b_{\pm}|^2 = \frac{\gamma^2}{\nu_{\pm}^2}\sin^2(\nu_{\pm}\ t). \tag{B.22b}$$

We see that, in the limit $\gamma \ll \omega_J, \omega_a$, and for $\omega_J \simeq \omega_a$, we have that $\gamma/\nu_+ \approx 0$ and $\gamma/\nu_- \approx 1$. So that $b_+ \approx 0$ and the transition probability takes the simple form

$$\rho_J^{11}(t) = |\alpha|^2\ \sin^2(\gamma t) \quad \text{and} \quad \rho_J^{11}(t) = p\ \sin^2(\gamma t), \tag{B.23}$$

in the first [Eq. (B.19)] and the second [Eq. (B.21)] case, respectively. In the second case, if $\rho_J(0) = |+\rangle\langle +|$, we obtain

$$\begin{aligned} \rho_J(t) &= \mathrm{Tr}_a\{\rho_{Ja}(t)\} \\ &= [p|a_+|^2 + (1-p)|a_-|^2]|+\rangle\langle +| + \\ &\quad +[p|b_+|^2 + (1-p)|b_-|^2]|-\rangle\langle -|. \end{aligned} \tag{B.24}$$

Thus, for $p \approx 0$, $\gamma \ll \omega_J, \omega_a$, and $\omega_J \simeq \omega_a$, we obtain

$$\rho_J^{11}(t) = \cos^2(\gamma t), \tag{B.25a}$$

$$\rho_J^{22}(t) = \sin^2(\gamma t), \tag{B.25b}$$

$$M_J^z(t) = \rho_J^{11}(t) - \rho_J^{22}(t) = \cos(2\gamma t), \tag{B.25c}$$

where $\rho_J^{22}(t) \equiv \langle -|\rho_J(t)|-\rangle$. Finally, it is worth pointing out that the symmetry property possessed by the Hamiltonian does not depend on the Hamiltonian parameters, but only on its structure. This implies that, even in the presence of time-dependent characteristic frequencies of the spins [$\omega_J(t)$ and $\omega_a(t)$], the reduction of the main two-spin dynamical problem to two independent effective single two-level dynamical problems remains valid.

References

[1] Benzi R, Parisi G, Sutera A, Vulpiani A. Stochastic resonance in climatic change. Tellus 1982;34(1):10–6.

[2] Gammaitoni L, Hänggi P, Jung P, Marchesoni F. Stochastic resonance. Rev Modern Phys 1998;70:223–87.

[3] Mantegna R, Spagnolo B. Stochastic resonance in a tunnel diode in the presence of white and colored noise. Nuovo Cimento D 1995;17(7–8):873–81. http://dx.doi.org/10.1007/BF02451845.

[4] Lanzara E, Mantegna RN, Spagnolo B, Zangara R. Experimental study of a nonlinear system in the presence of noise: the stochastic resonance. Amer J Phys 1997;65(4):341–9.

[5] Mantegna RN, Spagnolo B, Trapanese M. Linear and nonlinear experimental regimes of stochastic resonance. Phys Rev E 2000;63(1):011101.

[6] Spezia S, Curcio L, Fiasconaro A, Pizzolato N, Valenti D, Spagnolo B, et al. Evidence of stochastic resonance in the mating behavior of nezara viridula (l.). Eur Phys J B 2008;65:453–8. http://dx.doi.org/10.1140/epjb/e2008-00333-4.

[7] Mikhaylov A, Guseinov D, Belov A, Korolev D, Shishmakova V, Koryazhkina M, et al. Stochastic resonance in a metal-oxide memristive device. Chaos Solitons Fractals 2021;144:110723. http://dx.doi.org/10.1016/j.chaos.2021.110723.

[8] Valenti D, Fazio G, Spagnolo B. Stabilizing effect of volatility in financial markets. Phys Rev E 2018;97:062307. http://dx.doi.org/10.1103/PhysRevE.97.062307.

[9] Valenti D, Carollo A, Spagnolo B. Stabilizing effect of driving and dissipation on quantum metastable states. Phys Rev A 2018;97:042109. http://dx.doi.org/10.1103/PhysRevA.97.042109.

[10] Surazhevsky I, Demin V, Ilyasov A, Emelyanov A, Nikiruy K, Rylkov V, et al. Noise-assisted persistence and recovery of memory state in a memristive spiking neuromorphic network. Chaos Solitons Fractals 2021;146:110890. http://dx.doi.org/10.1016/j.chaos.2021.110890.

[11] Guarcello C, Valenti D, Spagnolo B. Phase dynamics in graphene-based Josephson junctions in the presence of thermal and correlated fluctuations. Phys Rev B 2015;92:174519. http://dx.doi.org/10.1103/PhysRevB.92.174519.

[12] Guarcello C, Valenti D, Augello G, Spagnolo B. The role of non-Gaussian sources in the transient dynamics of long Josephson junctions. Acta Phys Polon B 2013;44(5):997–1005. http://dx.doi.org/10.5506/APhysPolB.44.997.

[13] Grimaudo R, Valenti D, Spagnolo B, Filatrella G, Guarcello C. Josephson-junction-based axion detection through resonant activation. Phys Rev D 2022;105:033007. http://dx.doi.org/10.1103/PhysRevD.105.033007.

[14] Filatov DO, Vrzheshch DV, Tabakov OV, Novikov AS, Belov AI, Antonov IN, et al. Noise-induced resistive switching in a memristor based on ZrO2(Y)/Ta2O5 stack. J Stat Mech Theory Exp 2019;2019(12):124026. http://dx.doi.org/10.1088/1742-5468/ab5704.

[15] Valenti D, Denaro G, Cognata AL, Spagnolo B, Bonanno A, Basilone G, et al. Picophytoplancton dynamics in noisy marine environment. Acta Phys Polon B 2012;43(5):1227–40. http://dx.doi.org/10.5506/APhysPolB.43.1227.

[16] Lisowski B, Valenti D, Spagnolo B, Bier M, Gudowska-Nowak E. Stepping molecular motor amid Lévy white noise. Phys Rev E 2015;91:042713. http://dx.doi.org/10.1103/PhysRevE.91.042713.

[17] Ushakov YV, Dubkov AA, Spagnolo B. Regularity of spike trains and harmony perception in a model of the auditory system. Phys Rev Lett 2011;107:108103. http://dx.doi.org/10.1103/PhysRevLett.107.108103.

[18] Chichigina OA. Noise with memory as a model of lemming cycles. Eur Phys J B 2008;65(3):347–52. http://dx.doi.org/10.1140/epjb/e2008-00226-6.

[19] Hurbain J, Labavić D, Thommen Q, Pfeuty B. Theoretical study of the impact of adaptation on cell-fate heterogeneity and fractional killing. Sci Rep 2020;10:17429. http://dx.doi.org/10.1038/s41598-020-74238-y.

[20] Salahshour M, Rouhani S, Roudi Y. Phase transitions and asymmetry between signal comprehension and production in biological communication. Sci Rep 2019;9:3428. http://dx.doi.org/10.1038/s41598-019-40141-4.

[21] Melbinger A, Vergassola M. The impact of environmental fluctuations on evolutionary fitness functions. Sci Rep 2015;5:15211. http://dx.doi.org/10.1038/srep15211.

[22] Bennett M, Schatz MF, Rockwood H, Wiesenfeld K. Huygens's clocks. Proc R Soc Lond Ser A Math Phys Eng Sci 2002;458:563–79. http://dx.doi.org/10.1098/rspa.2001.0888.

[23] Wiesenfeld K. Spontaneous synchronization in large pendulum arrays. Eur Phys J Spec Top 2014;223:687–96. http://dx.doi.org/10.1140/epjst/e2014-02134-x.

[24] Strogatz SS, Stewart I. Coupled oscillations and biological synchronization. Sci Am 2014;269:102–9.

[25] Kapitaniak T, Kurths J. Synchronized pendula: From Huygens' clocks to chimera states. Eur Phys J Spec Top 2014;223:609–12. http://dx.doi.org/10.1140/epjst/e2014-02128-8.

[26] Blackburn JA, Marchese JE, Cirillo M, Grønbech-Jensen N. Classical analysis of capacitively coupled superconducting qubits. Phys Rev B 2009;79(5):054516.

[27] Grønbech-Jensen N, Marchese JE, Cirillo M, Blackburn JA. Tomography and entanglement in coupled Josephson junction qubits. Phys Rev Lett 2010;105:010501.

[28] Beck C. Possible resonance effect of axionic dark matter in Josephson junctions. Phys Rev Lett 2013;111:231801.

[29] Nenno DM, Garcia CA, Gooth J, Felser C, Narang P. Axion physics in condensed-matter systems. Nat Rev Phys 2020;2(12):682–96.

[30] Arvanitaki A, Dimopoulos S, Galanis M, Lehner L, Thompson JO, Van Tilburg K. Large-misalignment mechanism for the formation of compact axion structures: Signatures from the QCD axion to fuzzy dark matter. Phys Rev D 2020;101:083014.

[31] Battye RA, Garbrecht B, McDonald JI, Pace F, Srinivasan S. Dark matter axion detection in the radio/mm waveband. Phys Rev D 2020;102:023504.

[32] Braine T, et al. Extended search for the invisible axion with the axion dark matter experiment. Phys Rev Lett 2020;124:101303.

[33] Buschmann M, Foster JW, Safdi BR. Early-universe simulations of the cosmological axion. Phys Rev Lett 2020;124:161103.

[34] Co RT, Hall LJ, Harigaya K. Axion kinetic misalignment mechanism. Phys Rev Lett 2020;124:251802.

[35] Backes KM, et al. A quantum enhanced search for dark matter axions. Nature 2021;590(7845):238–42.

[36] Chaudhuri S. Impedance matching to axion dark matter: considerations of the photon-electron interaction. J Cosmol Astropart Phys 2021;2021(12):033.

[37] Nagano K, Nakatsuka H, Morisaki S, Fujita T, Michimura Y, Obata I. Axion dark matter search using arm cavity transmitted beams of gravitational wave detectors. Phys Rev D 2021;104:062008.

[38] Wang J-W, Bi X-J, Yin P-F. Detecting axion dark matter through the radio signal from omega centauri. Phys Rev D 2021;104:103015.

[39] Xiao Y, Wang H, Wang D, Lu R, Yan X, Guo H, et al. Nonlinear level attraction of cavity axion polariton in antiferromagnetic topological insulator. Phys Rev B 2021;104:115147. http://dx.doi.org/10.1103/PhysRevB.104.115147.

[40] Semertzidis YK, Youn S. Axion dark matter: How to see it? Sci Adv 2022;8(8):eabm9928. http://dx.doi.org/10.1126/sciadv.abm9928.

[41] Chadha-Day F, Ellis J, Marsh DJE. Axion dark matter: What is it and why now? Sci Adv 2022;8(8):eabj3618. http://dx.doi.org/10.1126/sciadv.abj3618.

[42] Irastorza IG. An introduction to axions and their detection. SciPost Phys Lect Note 2022;45. http://dx.doi.org/10.21468/SciPostPhysLectNotes.45.

[43] Alesini D, et al. Search for invisible axion dark matter of mass $m_a = 43\ \mu$eV with the QUAX–$a\gamma$ experiment. Phys Rev D 2021;103:102004.

[44] Salemi CP, et al. Search for low-mass axion dark matter with ABRACADABRA-10 cm. Phys Rev Lett 2021;127:081801. http://dx.doi.org/10.1103/PhysRevLett.127.081801.

[45] Reynolds CS, Marsh MCD, Russell HR, Fabian AC, Smith R, Tombesi F, et al. Astrophysical limits on very light axion-like particles from Chandra grating spectroscopy of NGC 1275. Astrophys J 2020;890(1):59. http://dx.doi.org/10.3847/1538-4357/ab6a0c.

[46] Dessert C, Foster JW, Safdi BR. X-ray searches for axions from super star clusters. Phys Rev Lett 2020;125:261102. http://dx.doi.org/10.1103/PhysRevLett.125.261102.

[47] Kohri K, Kodama H. Axion-like particles and recent observations of the cosmic infrared background radiation. Phys Rev D 2017;96:051701. http://dx.doi.org/10.1103/PhysRevD.96.051701.

[48] Moroi T, Nakayama K, Tang Y. Axion-photon conversion and effects on 21cm observation. Phys Lett B 2018;783:301–5. http://dx.doi.org/10.1016/j.physletb.2018.07.002.

[49] Caputo A, Sberna L, Frías M, Blas D, Pani P, Shao L, et al. Constraints on millicharged dark matter and axionlike particles from timing of radio waves. Phys Rev D 2019;100:063515. http://dx.doi.org/10.1103/PhysRevD.100.063515.

[50] Gramolin AV, Aybas D, Johnson D, Adam J, Sushkov AO. Search for axion-like dark matter with ferromagnets. Nat Phys 2021;17(1):79–84.

[51] Khlopov MY. Probes for dark matter physics. Internat J Modern Phys D 2018;27(06):1841013. http://dx.doi.org/10.1142/S0218271818410134.

[52] Sikivie P. Experimental tests of the "invisible" axion. Phys Rev Lett 1983;51:1415–7.

[53] Raffelt G, Stodolsky L. Mixing of the photon with low-mass particles. Phys Rev D 1988;37:1237–49. http://dx.doi.org/10.1103/PhysRevD.37.1237.

[54] Murayama H. Course 6 - Physics beyond the standard model and dark matter. In: Bernardeau F, Grojean C, Dalibard J, editors. Particle physics and cosmology: The fabric of spacetime. Les houches, vol. 86, Elsevier; 2007, p. 287–347. http://dx.doi.org/10.1016/S0924-8099(07)80032-1.

[55] Dixit AV, Chakram S, He K, Agrawal A, Naik RK, Schuster DI, et al. Searching for dark matter with a superconducting qubit. Phys Rev Lett 2021;126:141302.

[56] Devoret MH, Martinis JM, Esteve D, Clarke J. Resonant activation from the zero-voltage state of a current-biased Josephson junction. Phys Rev Lett 1984;53:1260–3.

[57] Guarcello C, Valenti D, Carollo A, Spagnolo B. Stabilization effects of Dichotomous noise on the lifetime of the superconducting state in a long Josephson junction. Entropy 2015;17(5):2862–75. http://dx.doi.org/10.3390/e17052862.

[58] Lee G-H, Efetov DK, Jung W, Ranzani L, Walsh ED, Ohki TA, et al. Graphene-based Josephson junction microwave bolometer. Nature 2020;586(7827):42–6. http://dx.doi.org/10.1038/s41586-020-2752-4.

[59] Walsh ED, Jung W, Lee G-H, Efetov DK, Wu B-I, Huang K-F, et al. Josephson junction infrared single-photon detector. Science 2021;372(6540):409–12.

[60] Braginski AI. Superconductor electronics: status and outlook. J Supercond Nov Magn 2019;32(1):23–44.

[61] Guarcello C. Lévy noise effects on Josephson junctions. Chaos Solitons Fractals 2021;153:111531. http://dx.doi.org/10.1016/j.chaos.2021.111531.

[62] Kuzmin LS, Sobolev AS, Gatti C, Di Gioacchino D, Crescini N, Gordeeva A, et al. Single photon counter based on a Josephson junction at 14 GHz for searching galactic axions. IEEE Trans Appl Supercond 2018;28(7):1–5.

[63] Guarcello C, Braggio A, Solinas P, Giazotto F. Nonlinear critical-current thermal response of an asymmetric Josephson tunnel junction. Phys Rev Appl 2019;11:024002. http://dx.doi.org/10.1103/PhysRevApplied.11.024002.

[64] Guarcello C, Braggio A, Solinas P, Pepe GP, Giazotto F. Josephson-threshold calorimeter. Phys Rev Appl 2019;11:054074.

[65] Revin LS, Pankratov AL, Gordeeva AV, Yablokov AA, Rakut IV, Zbrozhek VO, et al. Microwave photon detection by an Al Josephson junction. Beilstein J Nanotechnol 2020;11(1):960–5.

[66] Yablokov A, Glushkov E, Pankratov A, Gordeeva A, Kuzmin L, Il'ichev E. Resonant response drives sensitivity of Josephson escape detector. Chaos Solitons Fractals 2021;148:111058. http://dx.doi.org/10.1016/j.chaos.2021.111058.

[67] Piedjou Komnang A, Guarcello C, Barone C, Gatti C, Pagano S, Pierro V, et al. Analysis of Josephson junctions switching time distributions for the detection of single microwave photons. Chaos Solitons Fractals 2021;142:110496. http://dx.doi.org/10.1016/j.chaos.2020.110496.

[68] Guarcello C, Piedjou Komnang AS, Barone C, Rettaroli A, Gatti C, Pagano S, et al. Josephson-based scheme for the detection of microwave photons. Phys Rev Appl 2021;16:054015. http://dx.doi.org/10.1103/PhysRevApplied.16.054015.

[69] Pankratov AL, Revin LS, Gordeeva AV, Yablokov AA, Kuzmin LS, Il'ichev E. Towards a microwave single-photon counter for searching axions. npj Quantum Inf 2022;8(1):61. http://dx.doi.org/10.1038/s41534-022-00569-5.

[70] Pankratov AL, Gordeeva AV, Revin LS, Ladeynov DA, Yablokov AA, Kuzmin LS. Approaching microwave photon sensitivity with Al Josephson junctions. Beilstein J Nanotechnol 2022;13(1):582–9.

[71] Beck C. Possible resonance effect of dark matter axions in SNS Josephson junctions. PoS 2017;EPS-HEP2017:058.

[72] Hoffmann C, Lefloch F, Sanquer M, Pannetier B. Mesoscopic transition in the shot noise of diffusive superconductor–normal-metal–superconductor junctions. Phys Rev B 2004;70:180503.
[73] Bae M-H, Dinsmore III RC, Sahu M, Lee H-J, Bezryadin A. Zero-crossing shapiro steps in high-T_c superconducting microstructures tailored by a focused ion beam. Phys Rev B 2008;77:144501.
[74] Wang J, Wang Z, Wang P. Magnetic field enhanced critical current and subharmonic structures in dissipative superconducting gold nanowires. Quantum Front 2022;1(1):21. http://dx.doi.org/10.1007/s44214-022-00021-x.
[75] Krantz P, Kjaergaard M, Yan F, Orlando TP, Gustavsson S, Oliver WD. A quantum engineer's guide to superconducting qubits. Appl Phys Rev 2019;6:021318.
[76] Blais A, Grimsmo AL, Girvin SM, Wallraff A. Circuit quantum electrodynamics. Rev Modern Phys 2021;93:025005. http://dx.doi.org/10.1103/RevModPhys.93.025005.
[77] Grimaudo R, Messina A, Nakazato H. Exactly solvable time-dependent models of two interacting two-level systems. Phys Rev A 2016;94:022108. http://dx.doi.org/10.1103/PhysRevA.94.022108.
[78] Planat L, Ranadive A, Dassonneville R, Puertas Martínez J, Léger S, Naud C, et al. Photonic-crystal Josephson traveling-wave parametric amplifier. Phys Rev X 2020;10:021021. http://dx.doi.org/10.1103/PhysRevX.10.021021.
[79] McCumber DE. Effect of AC impedance on DC voltage-current characteristics of superconductor weak-link junctions. J Appl Phys 1968;39(7):3113–8.
[80] Barone A, Paterno G. Physics and applications of the Josephson effect. Wiley, New York; 1982.
[81] Guarcello C, Valenti D, Spagnolo B, Pierro V, Filatrella G. Anomalous transport effects on switching currents of graphene-based Josephson junctions. Nanotechnology 2017;28(13):134001. http://dx.doi.org/10.1088/1361-6528/aa5e75.
[82] Guarcello C, Valenti D, Spagnolo B, Pierro V, Filatrella G. Josephson-based threshold detector for Lévy-distributed current fluctuations. Phys Rev A 2019;11:044078. http://dx.doi.org/10.1103/PhysRevApplied.11.044078.
[83] Guarcello C, Filatrella G, Spagnolo B, Pierro V, Valenti D. Voltage drop across Josephson junctions for Lévy noise detection. Phys Rev Res 2020;2:043332. http://dx.doi.org/10.1103/PhysRevResearch.2.043332.
[84] Sikivie P, Yang Q. Bose-Einstein condensation of dark matter axions. Phys Rev Lett 2009;103(11):111301.
[85] Duffy LD, van Bibber K. Axions as dark matter particles. New J Phys 2009;11(10):105008.
[86] Bradley R, Clarke J, Kinion D, Rosenberg LJ, van Bibber K, Matsuki S, et al. Microwave cavity searches for dark-matter axions. Rev Modern Phys 2003;75:777–817.
[87] Grimaudo R, Vitanov NV, Messina A. Coupling-assisted Landau-Majorana-Stückelberg-Zener transition in a system of two interacting spin qubits. Phys Rev B 2019;99:174416. http://dx.doi.org/10.1103/PhysRevB.99.174416.
[88] Grimaudo R, Isar A, Mihaescu T, Ghiu I, Messina A. Dynamics of quantum discord of two coupled spin-1/2's subjected to time-dependent magnetic fields. Results Phys 2019;13:102147. http://dx.doi.org/10.1016/j.rinp.2019.02.083.
[89] Grimaudo R, Nakazato H, Messina A, Vitanov NV. Dzyaloshinskii-Moriya and dipole-dipole interactions affect coupling-based Landau-Majorana-Stückelberg-Zener transitions. Phys Rev Res 2020;2:033092. http://dx.doi.org/10.1103/PhysRevResearch.2.033092.
[90] Grimaudo R, Messina A, Sergi A, Vitanov NV, Filippov SN. Two-qubit entanglement generation through non-Hermitian Hamiltonians induced by repeated measurements on an Ancilla. Entropy 2020;22(10):1184. http://dx.doi.org/10.3390/e22101184.